The DOI for this manuscript is

DOI:10.2151/jmsj.2024-021

J-STAGE Advance published date: March 27th, 2024

Numerical Simulation on Feasibility of Rain Enhancement by Hygroscopic Seeding over Kochi Area, Shikoku, Japan, in Early Summer

Wei-Chen KUO, Katsuya YAMASHITA[*1]

Meteorological Research Institute, Japan Meteorological Agency, Tsukuba, Japan

Masataka MURAKAMI

Institute for Space-Earth Environmental Research, Nagoya University, Nagoya, Japan

Typhoon Science and Technology Research Center, Yokohama National University, Yokohama, Japan

Meteorological Research Institute, Japan Meteorological Agency, Tsukuba, Japan

Takuya TAJIRI, and Narihiro ORIKASA

Meteorological Research Institute, Japan Meteorological Agency, Tsukuba, Japan

Corresponding author: Masataka Murakami, Institute for Space–Earth Environmental Research, Nagoya University, Furo-cho, Chikusa-ku, Nagoya, Aichi 464-8601, JAPAN

Email: mamuraka@mri-jma.go.jp.

[*1] Current affiliation: Snow and Ice Research Center, National Research Institute for Earth Science and Disaster Resilience, Nagaoka, JAPAN

Abstract

In this study, we investigated the feasibility of rain enhancement by cloud seeding over a target area (Sameura Dam catchment area, Kochi Prefecture) in early summer. The effects of salt micro-powder (MP) and hygroscopic flare (HF) seeding on the initial cloud microphysical structures were investigated using a detailed bin microphysics parcel model with background atmospheric aerosol data collected from ground-based observations conducted on the windward side of the target area and seeding aerosol data collected from the coordinated flights of seeding helicopter and in-situ measurement aircraft. Numerical seeding experiments showed that the size distributions of cloud droplets were broadened, and the onset of raindrop formation was accelerated by MP and HF seeding, although MP seeding showed more notable seeding effects than did HF seeding. MP seeding increased the mean droplet size and decreased the total number concentration of cloud droplets, whereas HF seeding had the opposite effect. Based on the relationship between the increase/decrease ratio of the cloud droplet number concentration and increase/decrease ratio of the surface precipitation by hygroscopic seeding obtained in previous studies, MP seeding had a positive seeding effect, whereas HF seeding had a negative effect. In the numerical seeding experiments, a range of variations in the number concentration and hygroscopicity of background aerosol particles, updraft velocity near the cloud base, the amount of seeding material applied, and the change in the physicochemical properties of the seeding aerosols to improve seeding effects were also considered. However, the outline of the results described above remained unchanged. These results demonstrate the possibility

of increasing surface precipitation by MP seeding over the catchment. However, seeding a large amount of MP (NaCl) is necessary to enhance precipitation substantially. Simultaneously, considering the environmental impact is essential, as shown in our study.

Keywords: precipitation enhancement, warm cloud, hygroscopic seeding, salt micro-powder, hygroscopic flare

1. Introduction

Hygroscopic seeding is a technique potentially suitable for increasing precipitation from warm, convective clouds during summer. Hygroscopic particles less than 10 μm in diameter are seeded below the cloud base from an aircraft. The seeded particles, which are larger than the natural cloud condensation nuclei (CCN), prevent the smaller, natural CCN from nucleating into cloud droplets, resulting in a broader droplet spectrum and lower droplet number concentration at the cloud base. Furthermore, because there are fewer cloud droplets, they grow to larger sizes, often more efficiently by collision–coalescence with other smaller cloud droplets, initiating an early rain formation process within a typical cumulus cloud (Cooper et al. 1997). Results of hygroscopic seeding experiments in South Africa (Mather et al. 1997; Terblanche et al. 2000), Mexico (Bruintjes et al. 2003; World Meteorological Organization [WMO] 2000), Thailand (Silverman and Sukarnjanaset 2000), and the United States (Rosenfeld et al. 2010) suggested that hygroscopic seeding may be useful for rainfall enhancement and appear to be consistent with the numerical simulation results (Reisin et al. 1996; Yin et al. 2000; Segal et al. 2004), except for some details. Although these results are encouraging and intriguing, the effects of hygroscopic seeding remain poorly understood, and some fundamental questions, such as an effective size range and amount of seeding material, and a chain reaction of microphysical processes after seeding, remain unanswered. Consequently, the WMO (2000) stated that measurements of key steps in the chain of physical events associated with hygroscopic seeding are needed to confirm the conceptual seeding models and determine the range of effectiveness of seeding techniques in increasing precipitation from warm and mixed-phase convective clouds. There are two types of hygroscopic seeding materials: hygroscopic flare (HF) particles and salt micro-powder (MP) particles. The former is small salt particles (mainly made of submicron particles) produced from burning pyrotechnic flares, whereas the latter is hygroscopic salt powder milled to the optimal size (a few microns in diameter). Both materials are seeded in the updraft region at cloud base and introduced into the clouds with help of updraft. HF is currently widely used as a hygroscopic seeding material due to its ease of handling during seeding operation compared to MP.

To assess the feasibility of rain enhancement by hygroscopic seeding, understanding the physicochemical properties of background (BG) aerosol particles (APs) acting as CCN, cloud types suitable for cloud seeding, and their microphysical structures are essential (Bruintjes 1999; Kuba and Murakami 2010; Flossmann et al. 2019; Geresdi et al. 2021; Tessendorf et al. 2021). Kuba and Murakami (2010) suggested that the effect of hygroscopic seeding depends considerably on the cloud type and the atmospheric environment of cloud formation. Cotton (2009) indicated that the effect of hygroscopic seeding depends on the hygroscopicity, size, and concentration of BG APs and the seeding material.

To investigate the effects of hygroscopic seeding on cloud and precipitation, many studies have applied numerical models. Reisin et al. (1996), Yin et al. (2000), and Teller and Levin (2006) conducted numerical experiments to evaluate the role of hygroscopic seeding using an axisymmetric or a two-dimensional slab-symmetric, non-hydrostatic cloud model with a bin spectral microphysical scheme and showed the effectiveness of hygroscopic seeding for rain enhancement. However, in their models, grid sizes ranged from 150–300 m in the vertical direction, which is not fine enough to estimate the maximum supersaturation that significantly affects CCN activation.

Cooper et al. (1997), Caro et al. (2002), and Segal et al. (2004) investigated the effect of HF seeding using a parcel model with a precise microphysical model and suggested that rain formation via the collision–coalescence process can be accelerated significantly by hygroscopic seeding. However, estimation of surface rainfall using parcel models appears to be inaccurate due to their intrinsic limitation. Kuba and Murakami (2010) provided a more detailed review of previous studies and their insufficiencies.

In most of the studies mentioned above, the expression of the competitive effect for available water vapor among BG and seeding aerosols and the evaluation of the tail effect, where a few large hygroscopic particles grow to large droplets faster and start a collection of small cloud droplets, were insufficient. In addition, both BG and seeding aerosols were simplified rather than based on actual measurements, such that those simulation results cannot be considered as definitive evaluations of the effects of MP and HF seeding. Reflecting this research background, several precipitation enhancement projects using HF have been carried out since then, and HF is still used in some projects today.

However, because HF generates high concentrations of submicron hygroscopic particles and produces high concentrations of small cloud droplets, doubts rose about its rain enhancement effect (Kuba and Murakami 2010, Rosenfeld et al. 2010). Subsequently, field experiments were conducted to confirm the effectiveness of MP against HF (Rosenfeld et al. 2010, Murakami et al. 2015); no definitive conclusions could be drawn, although the superiority of MP over HF was suggested.

Recently Tessendorf et al. (2021) and Geresdi et al. (2021) investigated the effect of hygroscopic seeding using parcel models with bin spectral microphysical schemes. In the model used by Tessendorf et al. (2021), the collision–coalescence was excluded; instead, a moving-bin method was employed to calculate the evolution of the droplet size distributions (DSDs) precisely. They evaluated the hygroscopic flare seeding effect on the initial cloud DSD using the BG aerosol observed in southeastern Queensland, Australia, together with the seeding aerosol size distributions and made a comparison with the observed initial cloud DSD. In the model used by Geresdi et al. (2021), within 100 m above the cloud base, the evolution of the DSDs was accurately calculated using a moving-bin method and the collision–coalescence was excluded. The curvature and solution effects on condensational growth of solution droplets were taken into consideration. They also used the BG aerosol size distributions observed in southeastern Queensland, Australia, and the United Arab Emirates mountain area, and investigated the sensitivity of initial cloud DSDs to the properties of seeding aerosols. However, both studies did not assess the seeding effect on surface precipitation due to the intrinsic limitation of parcel models.

Kuba and Murakami (2010) performed idealized seeding simulations using a two-dimensional kinetic model implemented with a detailed cloud microphysics scheme and revealed that increasing rainfall by a maximum of 20% using the salt micro-powder cloud seeding method was possible. The key change in microstructures owing to hygroscopic seeding for the enhancement of total surface precipitation is an increase in the mean droplet size and a decrease in the total droplet number concentration (Kuba and Murakami 2010, 2012). They calculated the activation of CCN in a Lagrangian manner, the subsequent condensational growth and collision–coalescence process in a semi-Lagrangian manner, and the fall of particles in an Eulerian manner, and sought to evaluate as accurately as possible the hygroscopic seeding effects via changes in microphysical properties on surface precipitation. However, there was still insufficient accuracy in calculating the competition for available water vapor among BG and seeding aerosols and the tail effect in early onset of the collection of small droplets by large droplets; the size of swollen droplets formed from giant CCN particles was evaluated using an approximate formula and the solution effect on the condensational growth of cloud droplets immediately after activation was ignored. Furthermore, the characteristics of the BG and seeding aerosols were not based on actual measurements, but simplified ones.

The Meteorological Research Institute of the Japan Meteorological Agency, in cooperation with 10 other research organizations, carried out the five-year research project (2006–2011) “Japanese Cloud Seeding Experiments for Precipitation Augmentation” (JCSEPA) to realize drought mitigation and water resources management (Murakami and JCSEPA Research Group 2011; Murakami et al. 2015). The project had two goals: to sophisticate weather modification technology for orographic snow clouds and to investigate the possibility of rain enhancement by hygroscopic seeding for cumulus and stratocumulus clouds in warm seasons. The study on hygroscopic seeding was carried out targeting warm clouds in Shikoku, southwestern part of Japan, using cloud simulation chamber experiments, numerical model simulations, ground-based aerosol measurements, x-, ka-, and w-band radar measurements, dual-frequency depolarization lidar measurements, multi-wavelength microwave radiometer measurements, and aircraft seeding experiments. Fujibe et al. (2008) reported that the Sameura Dam, the main water supply for Shikoku, located in central Shikoku, with a mean annual precipitation amount exceeding 3,000 mm, has recently experienced frequent, severe water shortages because of a large year-to-year variation in summer precipitation. Koshida et al. (2012) investigated the occurrence frequency and types of clouds suitable for cloud seeding in summer in Shikoku using operationally available data, such as Multifunctional Transport Satellite and Radar-AMeDAS (Automated Meteorological Data Acquisition System) precipitation data. They reported that the chance for artificial rainfall augmentation to secure water resources (as a preventive measure against droughts) was estimated to exist in at least 17% of total time in the warm season, as derived from the sum of "warm clouds" (for hygroscopic seeding) and "cold clouds" (for glaciogenic seeding) in dry months. Approximately half of the clouds that could potentially increase rainfall through seeding were warm clouds with cloud top temperatures of -5 °C or higher (with approximate cloud top heights of 6 km or less), making them suitable for hygroscopic seeding.

In the JCSEPA project, we performed ground-based measurements in Kochi city, windward of the area chosen as a target for precipitation enhancement (Sameura Dam in Shikoku), during June 2010, synchronized with instrumented aircraft observations to investigate the physicochemical properties of BG APs that would function as CCN. The observation results showed that the mean concentrations of APs and CCN were considerably affected by air pollution. Even air masses from the Pacific Ocean were considerably affected by air pollution in East Asia, including Japan.

In this study, the insufficient accuracy in calculating the competition and the tail effects by Kuba and Murakami (2010) was improved using a modified, detailed bin microphysics parcel model (Misumi et al. 2010; Yamashita et al. 2011) based on the model proposed by Chen and Lamb (1994), where the swelling (water vapor absorption) of hygroscopic particles, including giant CCN particles, the competition for available water vapor among BG and seeding aerosols, their activation as CCN, and subsequent condensation and collision–coalescence growth leading to the formation of raindrop embryos could be more accurately calculated. Using the parcel model initialized with atmospheric and environmental conditions observed over the Kochi area, Japan, in the early summer of 2010, the effects of MP and HF seeding on initial cloud microstructure were simulated. From the relationship between cloud droplet number concentration immediately after CCN activation just above the cloud base and surface precipitation, which was obtained from Kuba and Murakami's simulation results (Tables 2 and 4 of Kuba and Murakami, 2010) using various seeding aerosols and the change in cloud droplet number concentration with and without hygroscopic seeding obtained from this study, we evaluated the hygroscopic seeding effects on surface precipitation. Based on the simulation results, the feasibility of rain enhancement by hygroscopic seeding was discussed, focusing on the advantage of MP compared to HF, the condition that the disadvantage of HF could be negligible, and the impacts of the hygroscopic seeding according to the experimental setup obtained from the in-situ measurement targeting Kochi area as part of JCSEPA project.

2. Background and hygroscopic seeding aerosols

Regarding background aerosols, since data collected from ground-based observations were shown to be representative of aerosol data within the boundary layer collected from in-situ aircraft measurements (Yamashita et al. 2023), daytime aerosol data collected during the observation period from June 6–24, 2010, were used. Considering the variations in aerosol number concentration, the median value (bimodal), 90th percentile value (bimodal), and 10th percentile value (bimodal) of the measured aerosol size distributions were used as those of the background aerosols, and each aerosol size distribution was approximated by the superimposition of multiple log-normal distributions (Fig. 1). The hygroscopicity, κ, of the background aerosol was assumed to be a mean value of 0.1, obtained from observations (Yamashita et al. 2023). Considering the variation range (standard deviation) in the observed hygroscopicity, we also conducted sensitivity experiments of seeding effects on hygroscopicity, using 0.03 and 0.3 hygroscopicity.

The size distributions of the MP and HF particles were based on data obtained from coordinated flights of the seeding helicopter and the in-situ measurement aircraft (Fig. 2). These results were mostly consistent with those obtained from laboratory experiments in which MP was generated using a rotating brush disperser (Palas GmBH, model RBG-1000), and HF was burned in a high-speed wind tunnel.

NaCl particles mixed with anti-caking agents ($CaCO_3$ and SiO_2 particles) used in actual seeding experiments were assumed for MP seeding experiments. The MP was developed in the JCSEPA project and comprised NaCl particles with a log-normal size distribution (modal diameter of 2.6 μm and geometric dispersion of 0.8), $CaCO_3$ particles with a log-normal size distribution (modal diameter of 2.6 μm and geometric dispersion of 0.8), and SiO_2 particles with a log-normal size distribution (modal diameter of 0.1 μm and geometric dispersion of 0.82). $CaCO_3$ and SiO_2 particles were included at 2% and 3% of total weight as anti-caking agents to prevent aggregation and enable fluidity of MP. The hygroscopicities of the three particle types were 1.2, 0.01, and 0.01, respectively. In addition, to investigate the adverse effects of anti-caking agents on the seeding effect, MP particles represented by a mono-modal, log-normal distribution consisting of pure NaCl were examined.

HF is manufactured by ICE Inc. in the United States, and the particles (combustion products) are a mixture of mainly KCl and $CaCl_2$. Therefore, it was treated as a bimodal size distribution approximated by a combination of two log-normal distributions with different modal diameters of 0.1 and 0.3 μm (Fig. 2). Assuming the same hygroscopicity for the APs belonging to the two modes, the simulation was performed by setting the hygroscopicity to 0.6, which was experimentally obtained for APs smaller than 0.1 μm (Tajiri et al. 2020). As a sensitivity experiment, simulations were performed assuming a hygroscopicity of 1.1 for pure KCl.

3. Simulations of hygroscopic seeding

3.1 Model description

To investigate the effects of hygroscopic seeding on the initial microphysical structures of clouds, the deliquescence, swelling, and activation of CCN particles and the subsequent condensation and collision–coalescence growth of cloud droplets during adiabatic ascent were simulated using a detailed double-moment (mass and number of APs / cloud droplets in each bin) and multi-dimensional (three dimensions to represent water droplet properties: water, soluble aerosols, and insoluble aerosols; five dimensions to represent ice particle properties: ice, soluble aerosol, insoluble aerosols, aspect ratio, and volume) bin microphysics parcel model. The equations of warm rain microphysical processes used in the parcel model were similar to those of Chen and Lamb (1994), except for the implementation of the κ-Köhler theory of Petters and Kreidenweis (2007), rather than the classical Köhler theory (Yamashita et al. 2011). In the current study, we applied two bin components (water and solute mass) to the liquid-phase framework. The two components were calculated simultaneously and independently to accurately calculate the curvature and solution effects on the condensational growth of cloud droplets. This allows a more realistic simulation of the competition for available water vapor among water drops containing different CCN particles of different sizes that can be accurately calculated.

The double-moment bin scheme and hybrid bin method allowed us to calculate the evolution of droplet spectra as accurately as possible and suppress numerical diffusion (see Chen and Lamb 1994 for detail).

The fallout of water droplets from the parcel was not considered, assuming that the droplet fluxes falling into the parcel from above and falling out from the parcel downward are approximately balanced, and the vertical advection term of droplets is negligibly small. For simplicity, the entrainment mixing of the parcel was not considered.

Water mass was divided into 72 bins ranging from 4.19×10^{-26} kg (2.155×10^{-10} m radius) to 7.55×10^{-8} kg (2.622×10^{-4} m radius) and aerosol mass was divided into 72 bins ranging from 9.79×10^{-25} kg (5.093×10^{-10} m radius) to 1.32×10^{-4} kg (2.613×10^{-3} m radius). The lower bin limits of successive larger bins were defined as $m_{i+1} = q_i\, m_i$, where q is the bin-sizing factor determined by $q_{i+1} = q_i / \theta$ (see Table 1 for details). Time integration was performed until the parcel reached a height of 1,000 m, according to the description in Section 3.2. The time step used for the calculation was 0.1 s.

3.2 Configuration of seeding experiment

The initial parcel conditions were 23.3 °C, 1011.6 hPa, and 80% relative humidity (RH). These were the mean values observed in June 2010 at the Kochi Local Meteorological Observatory. The parcel was lifted at speeds of 0.5, 1, and 2 m s^{-1}, which were within the range of typical values obtained from aircraft observations just below the cloud bases.

The model simulated the cumulus cloud, whose base was approximately 480 m, and stopped at approximately 500 m above the cloud base because we focused on the seeding effect on the processes leading to the formation of raindrop embryos from a pure microphysics perspective. In the hygroscopic seeding simulation, the air parcel that included the BG APs and the seeding particles was adiabatically lifted at a constant ascent velocity. Therefore, the initial size distribution of the aerosol particles in the seeded case was assumed to be the sum of the size distributions of the BG APs and seeding particles. Because the model used here could not handle multiple aerosol types with different hygroscopicities, we shifted the size distribution of BG APs with a hygroscopicity of 0.1 toward smaller sizes to have modal sizes corresponding to the same critical supersaturations for seeding particles with a hygroscopicity of 1.2 for MP or 0.6 for HF particles (Fig. 3). Figure 4 shows the DSDs 20 s (a) and 200 s (b) after the activation point obtained from the parcel model simulation using the two size distributions shown in Fig. 3. The two sets of DSDs, shown as black and red lines, are almost identical, which means that the DSD activated from BG APs with original size distribution and κ = 0.1 are reproduced by BG APs with the shifted size distribution and κ = 1.28.

4. Results

4.1 Salt micro-powder seeding

Figure 5 shows the initial CCN size distributions and DSDs at 500 and 600 m obtained from the model simulation using the size distribution shown in Fig. 5a for the MP case and an updraft velocity of 1.0 m s^{-1}. As the size distributions of the MP and HF particles were measured immediately after dispersal from the seeding helicopter and their concentrations were very high, simulations were also conducted at 10- and 100-fold diluted concentrations. The DSDs at 500 and 600 m for the seeded cases were broader than those for the unseeded case. The degree of broadening of the DSD increased with the number of seeding particles.

Figure 6 shows the time series of RH, condensation nuclei concentration (number concentration of total APs not activated yet), cloud droplet concentration ($5 < D < 100$ μm), and raindrop concentration ($D > 100$ μm) obtained from the model simulations shown in Fig. 5. The loss terms related to the change in CN concentration just before and after activation as CCN (near the cloud base height), are nucleation scavenging (activation as CCN) and in-cloud scavenging. The change in CN concentrations is mostly determined by the former. The cloud droplet number concentration is determined by the cloud droplet formation due to CCN activation and the loss term due to collision–coalescence, with the former overwhelmingly dominant. Therefore, the time series of CN concentration and the time series of cloud droplet number concentration show a mirror image relationship (Fig. 6). This also holds true for HF seeding (Fig. 9).

Notably, the raindrop concentration line for the unseeded case appeared marginally at approximately 900 m. The appearance time and number of raindrops for the seeded case were much earlier, even earlier than when RH reached 100%, and higher than those for the unseeded case.

Raindrop formation is thought to occur through the collision–coalescence and condensational growth processes, which generally work at the same time. Once the number of droplets close to 100 μm increases, raindrop formation is dominated by the condensational growth. However, in the case of MP seeding, very few giant MP particles swell and rapidly grow to solution drops close to 100 μm and start collecting smaller solution droplets, forming solution drops larger than 100 μm even before RH reaches 100%. While reaching RH of 100%, a considerable number of solution droplets close to 100 μm became raindrop-size through condensational growth. Since the cloud droplet number concentration was low, due to the synergistic effect of efficient condensational growth of large solution droplets and inactive collision–coalescence, raindrop formation through condensational growth continued to dominate (Fig. 7).

When MP particles were added to the BG APs, the raindrop concentration was similar to that in the MP-only case. The simulation results that the size distribution and total number concentration of droplets in the size range larger than 10 μm and the time evolution of the RH for the MP-only case were similar to those for the BG APs plus MP case (Figs. 5 and 6) indicate that the raindrops were predominantly produced through the collision–coalescence process of large solution droplets grown from the seeded MP particles. As observed in the DSD at 500 m in Fig. 5, the formation of cloud droplets smaller than 10 μm activated from BG APs was suppressed by the lowered water supersaturation (SSw) owing to the condensational growth of large and hygroscopic MP particles, and the corresponding moisture condensed on the large solution droplets formed on MP particles (the competition effect). As shown in the time series of RH in Fig. 6, the onset of SSw rise was delayed, and the maximum SSw was suppressed owing to water vapor condensation on the MP particles. However, the main raindrop formation mechanism was the collision–coalescence of large droplets grown through water vapor condensation from the MP particles (the tail effect).

In comparison, when the MP particles were diluted 10 or 100 times to lower concentrations, the effect of suppressing the formation of cloud droplets smaller than 10 μm and promoting the growth of large solution droplets (competitive effect) became weaker. Nevertheless, raindrops were generated by the collision–coalescence of large solution droplets formed on MP particles; however, their number concentration was low and only advanced the onset of raindrop formation, which did not lead to a significant increase in precipitation. These results demonstrate the effects of MP seeding from the perspective of cloud microphysics. From these results, the rain enhancement is possible by seeding the right amount of MP over the Kochi area.

4.2 Hygroscopic flare seeding

Figures 8 and 9 are similar to Figs. 5 and 6, respectively, except for the HF seeding case. The DSDs at 500 and 600 m for the HF-seeded case were broader than those for the unseeded case, similar to the MP-seeded case. The appearance time and number of raindrops for the HF-seeded case were also earlier and higher than those for the unseeded case, similar to the MP-seeded case. However, the broadening of the DSD and the number of raindrops were less remarkable compared to the MP case. Unlike the MP case, in the HF case, cloud droplets activated on majority of HF particles and some large BG APs gradually grew and shifted to larger sizes by condensation and collision–coalescence growth, with raindrops larger than 100 μm slowly forming after 600 s. Finally, a considerable number of cloud droplets close to 100 μm became raindrop-size through condensational growth (Fig. 10).

HF seeding also reduced SSw; however, this was due to the addition of HF particles to the BG APs, which increased the number of particles that acted as CCN and increased the amount of water vapor condensation. The reduction of

SSw by HF seeding suppressed the activation of smaller particles contained in the second mode of BG APs; however, more particles in the second mode of HF particles, which had higher concentrations, slightly larger sizes, and higher hygroscopicity than those of BG APs in their second mode, were activated. Consequently, the total concentration of cloud droplets substantially increased, and the mean droplet size substantially decreased. According to Kuba and Murakami (2010, 2012), these changes in microphysics properties would suppress total precipitation.

5. Discussion

5.1 BG AP concentration dependency of the seeding effect

For MP seeding, the higher the BG AP number concentration, the greater the seeding effect, which reduces the cloud particle number concentration. However, the seeding effect of the HF, which increases the cloud droplet number concentration, becomes more conspicuous with decreasing BG AP number concentration, although this causes a negative seeding effect in terms of precipitation enhancement, as will be discussed later. Therefore, MP and HF seedings were more effective with increasing amounts of seeding material in varying (increase/decrease) cloud droplet number concentrations (Table 2).

MP seeding showed no substantial effect when MP particles were diluted 10- and 100-fold. However, HF seeding showed some significant effects even when HF particles were diluted 10 and 100 times, although HF seeding led to a negative effect in precipitation enhancement.

From the perspective of precipitation enhancement, the cloud droplet number concentration decreased to approximately 50% of the unseeded case when high concentrations (measured in the seeding plume) of MP were seeded. According to Kuba and Murakami's (2010, 2012) relationship between cloud droplet number concentration ratio and total precipitation ratio for seeded and unseeded cases, rainfall from warm convective clouds is expected to increase by approximately 20%.

5.2 BG AP hygroscopicity dependency of the seeding effect

In the standard experiments described in Section 4, the hygroscopicity of the BG APs was assumed to be 0.1, which was the mean value averaged over all particle sizes obtained from ground-based observations (Yamashita et al. 2023). Since its variation was large, seeding simulations (assuming κ = 0.03 and 0.3 when considering the observed variation range) were also performed.

The results showed that the MP seeding effect on the droplet concentration ratio did not change considerably with decreasing BG AP hygroscopicity, whereas the HF seeding effect increased markedly with decreasing BG AP hygroscopicity (Table 3). However, this led to the suppression of surface precipitation.

5.3 Updraft velocity dependency of the seeding effect

For MP and HF seeding, the number concentrations of activated cloud droplets increased with increasing updraft velocity near the cloud base; however, the effect of updraft velocity on the droplet concentration ratio of the seeded and unseeded cases was different between MP and HF seeding (Table 4). For MP, the seeding effect weakened as the updraft strengthened. This is because the stronger the updraft velocity, the weaker the effect of suppressing the increase in RH before activation, owing to the swelling of MP particles, resulting in a higher SSw and activation of more BG APs with smaller sizes. However, for HF, the seeding effect did not vary with the strength of the updraft as much as it did in the MP case. This is because the stronger the updraft, the higher the SSw, which activates smaller BG AP and HF particles in the seeded case but also activates smaller BG AP particles in the unseeded case. Consequently, changes in the droplet number concentration ratio were relatively offset, and large changes in the seeding effect were suppressed.

5.4 Effect of anti-caking agents of MP

As mentioned above, in actual MP seeding, from the viewpoint of operability, $CaCO_3$ particles with a modal diameter of 2.6 μm and SiO_2 particles with a modal diameter of 0.1 μm were mixed at a 2% and 3% weight ratio, respectively, as anti-caking agents. The results of MP seeding experiments with and without anti-caking agents were compared to investigate the extent to which these anti-caking agents reduced the seeding effect.

The MP made of pure NaCl particles without anti-caking agents had a slightly larger seeding effect compared to the MP with anti-caking agents, but the difference was negligible, regardless of the BG AP concentration (Table 5).

5.5 Possibility of improving seeding effect by HF

HF was developed in South Africa in the 1990s (Mather et al. 1997) as an atomization technology for hygroscopic particles. HF is currently used in several projects worldwide because of its superior operability during seeding compared with MP. However, thus far, the high concentration of hygroscopic particles of approximately 0.1 μm contained in the second mode, produces high concentrations of cloud droplets, which leads to a negative seeding effect from the perspective of promoting the warm rain process and increasing precipitation. Therefore, we changed the properties of the HF particles by trial and error to determine how to improve them to obtain a positive seeding effect while maintaining the operability of the HF (Table 6).

First, comparing the case for the hygroscopicity of the HF particles with a pure KCl value of κ = 1.1 with the previous case of κ = 0.6, shown in Section 4.2., there is still a negative seeding effect and no significant improvement, even with κ = 1.1.

Next, the number concentration of hygroscopic particles in the second mode was reduced. As an extreme example, the hygroscopic particle number concentration in the second mode was set to zero. As a result, the seeding effect weakened but still showed a negative seeding effect for the 10th percentile value of the size distribution (LOW BG AP case), while showing a slight positive effect for the MID and HIGH BG AP cases.

Finally, seeding experiments were performed by increasing first modal diameters from 0.3 μm to 0.5, 1.0, and 2.0 μm, while keeping the hygroscopic particle number concentration in the second mode as zero. The results indicated that the seeding effect became positive (increase in precipitation) when the modal diameter was 0.5 μm or larger. This result is consistent with previous study results

(Cooper et al. 1997, Yin et al. 2000, Caro et al. 2002, Segal et al. 2004, Kuba and Murakami 2010, Geresdi et al. 2021), showing that hygroscopic particles larger than 1 μm in diameter have a positive seeding effect.

We established that unless the modal diameter of the first mode of hygroscopic particles generated from HF increased to 0.5 μm or larger (specifically, hygroscopic particles in the first mode include a substantial number of particles larger than 1 μm) and the number concentration of hygroscopic particles of approximately 0.1 μm contained in the second mode was largely reduced, HF seeding did not lead to a positive seeding effect, which aims to promote the warm rain process and increase surface precipitation.

5.6 Rough estimate of precipitation enhancement by MP seeding and required amount of seeding material

In this sub-section, we estimated the amount of MP seeding material required to enhance a seasonal precipitation by 20% based on the mass concentration of seeding aerosols required to halve the cloud droplet number concentration by hygroscopic seeding obtained from the results of this study and the 20% increase in seasonal precipitation by halving the cloud droplet number concentration obtained from the numerical simulation of Murakami et al. (2015), using a three-dimensional (3D), non-hydrostatic model.

In this study, we showed that under the condition of average BG AP number concentration, when high concentrations of MP particles (mass concentration of 5 mg m^{-3} estimated from particle size distribution in the plume immediately after seeding shown in Fig. 2) were seeded, cloud droplet number concentration was approximately halved. The result of MP seeding experiments during the 2008 warm season using a 3D, non-hydrostatic model incorporating double-moment cloud microphysics parameterization, where the MP seeding effect is simulated by halving CCN number concentration (cloud droplet number concentration to be activated at cloud base), showed a seasonal precipitation increase of approximately 20% (Murakami et al. 2015). This relationship between cloud droplet number concentration ratio and total precipitation ratio of seeded and unseeded cases is consistent with that obtained by Kuba and Murakami (2010, 2012).

We estimated the order of magnitude of MP particle mass required to increase precipitation by 20%. Here, we assumed that the dam's catchment area was 20 km × 20 km and that the rainfall in one season increased from 1,000 mm to 1,200 mm by seeding. The average rainfall of 1,000 mm in the catchment area corresponded to $(2 \times 10^4)^2$ m^2 × 1 m = 4×10^8 m^3 = 400 million tons of water. If the cloud physical precipitation efficiency (precipitation amount/amount of water vapor flowing into the cloud from the cloud base) was 0.2, 2×10^9 m^3 of water vapor flowed from the cloud base. Assuming a cloud base temperature of 18.5 °C and atmospheric pressure of 950 hPa, the density of water vapor in the air mass flowing into the cloud from the cloud base was approximately 1.6×10^{-2} kg m^{-3}. Therefore, the calculated volume of the air parcel flowing into the cloud from the cloud base was 1.25×10^{14} m^3. Because the mass concentration of MP particles in the air is approximately 5×10^{-6} kg m^{-3} to obtain a seeding effect of 20% increase in surface precipitation, the total amount of MP particles seeded in one season could be 6.25×10^8 kg (6.25×10^5 tons), which means that MP (NaCl) particles can be sprayed at 1.6 kg m^{-2} a season.

In nature, the amount of sea salt (NaCl) particles that fall on areas near the ocean is estimated to be in the order of 0.1 kg m^{-2} y^{-1} as a total of wet and dry depositions. Therefore, the amount of MP particles required to increase rainfall by 20% necessitates considering the environmental impact.

Since the seeding effect also depends on the characteristics of BG APs, strictly speaking, the estimation made here is valid for this target area. However, even considering the range of variation in the observed BG AP characteristics, this estimate almost holds true, indicating that in order to obtain a substantial increase in seasonal precipitation by MP seeding in areas other than the target area of this study, a huge amount of hygroscopic particles would be required, and environmental impact cannot be ignored.

6. Conclusion

The effects of MP and HF seeding on the initial cloud microphysical structure were investigated using a detailed bin microphysics parcel model to examine the feasibility of precipitation enhancement by hygroscopic seeding over a target area (Sameura Dam catchment area) in early summer under realistic conditions.

The physicochemical properties of the BG APs, which are part of the input data for the numerical seeding experiment, were obtained from ground-based observations conducted in Kochi city in June 2010. Another part of input data, the physicochemical properties of the hygroscopic seeding particles, was obtained from coordinated flights of the seeding helicopter and an in-situ measurement aircraft.

Numerical seeding experiments conducted under realistic atmospheric/environmental and seeding conditions showed that MP and HF seeding broadened the size distributions of cloud droplets to larger sizes and accelerated the onset of raindrop formation compared with unseeded cases. However, MP seeding yielded more remarkable seeding effects than HF seeding. MP seeding showed a substantial increase in mean droplet size and a decrease in the total number concentration of cloud droplets, whereas HF seeding showed the opposite effect. According to the relationship between the increase/decrease ratio of cloud droplet number concentration and the increase/decrease ratio of total precipitation due to hygroscopic seeding in previous studies (Kuba and Murakami 2010, 2012), MP seeding has a positive seeding effect and HF seeding has a negative effect.

In the numerical seeding experiments, the range of variation from the mean values for the number concentration and hygroscopicity of BG APs and updraft velocity near the cloud base, the amount of seeding material applied, and the change in the physicochemical properties of the seeding material for the improvement of seeding effects were considered. Most of the results described above remained the same although there were slight quantitative differences in the seeding effect.

These results indicate the feasibility of increasing surface precipitation by MP seeding in the target area. However, large amounts (5 mg m^{-3}) of MP (NaCl) particles need to be applied to the inflow air into clouds to yield a substantial (20%) increase in precipitation. In addition, if MP seeding is conducted throughout a season, its environmental impact must be considered because more NaCl particles, compared to the amount of sea salt particles deposited in the coastal area by dry and wet deposition, would fall on the ground.

HF is currently used as a hygroscopic seeding material around the world due to its ease of handling during seeding operation compared to MP. However, as shown in this paper, generating a large number of particles with small sizes (modal diameter of approximately 0.1 μm) causes an increase in the total number of cloud droplets, a decrease in the mean droplet size, and the suppression of a collision–coalescence process, which results in a decrease in surface precipitation. To obtain a positive seeding effect while maintaining the operability of HF, it is necessary to make the first (large size) mode particles surpass the second mode particles in both mass and number concentrations and also increase the modal diameter over 1.0 μm.

In this study, we used the results of the parcel model to qualitatively touch on the differences between MP and HF seeding in the timing of raindrop embryo formation and their number concentration. However, owing to the intrinsic limitations of parcel models, it is not possible to accurately evaluate the raindrop formation process. Therefore, in this study, we combined the results of Kuba and Murakami (2010, 2012) and the results of this study to evaluate the increase or decrease in surface precipitation due to MP and HF seeding via the cloud droplet number concentration activated near the cloud base and assessed their effectiveness. However, the validity of this method is limited to the range of hygroscopic seeding that has been carried out for warm clouds in the previous study and is not suitable for evaluating the seeding effect for a wider range of cloud types including mixed-phase clouds and wider range of seeding aerosol properties. In order to evaluate the effects of hygroscopic seeding targeting a wider range of cloud types under realistic atmospheric conditions, it is desirable to develop a 3D cloud resolving model that incorporates schemes that can accurately calculate the competition for available water vapor between multiple aerosol species (through accurate CCN aerosol swelling, activation, and subsequent condensational growth), the collision–coalescence process between cloud droplets, and the various cold rain processes. The effectiveness of various hygroscopic seeding methods should be assessed through numerical experiments using such a model.

Data Availability Statement

The numerical simulation data analyzed in this study are available from the corresponding author on request.

Acknowledgments

This study was partly supported by the Ministry of Education, Culture, Sports, Science, and Technology of the Japanese Government under the program of Special Coordination Funds for Promoting Science and Technology, JCSEPA. This work was also partly supported by Japan Society for the Promotion of Science KAKENHI (Grant Numbers 23244095 and 17H00787) and Japan Science and Technology Agency Moonshot Research and Development (Grant Number JPMJMS2282-04).

References

Bruintjes, R. T., 1999: A review of cloud seeding experiments to enhance precipitation and some new prospects. *Bull. Amer. Meteor. Soc.*, **80**, 805-820.

Bruintjes, R. T., D. W. Breed, G. B. Foote, V. Salazar, M. J. Dixon, T. Fowler, and B. G. Brown, 2003: Program for the augmentation of rainfall in Coahuila: Overview and results. *Proceedings of the Eight WMO Scientific Conference on Weather Modification*, April 2003, Casablanca, Morocco, 103-106.

Chen, J.-P., and D. Lamb, 1994: The theoretical basis for the parameterization of ice crystal habits: Growth by vapor deposition. *J. Atmos. Sci.*, **51**, 1206-1222.

Cooper, W. A., R. T. Bruintjes, and G. K. Mather, 1997: Calculations pertaining to hygroscopic seeding with flares. *J. Appl. Meteor.*, **36**, 1449-1469.

Cotton W. R., 2009: Parallels and contrasts between deliberate cloud seeding and aerosol pollution effects. *Aerosol Pollution Impact on Precipitation: A Scientific Review.* Z. Levin and W. R. Cotton, Eds., Springer, 277-294.

Flossmann, A. I., M. Manton, A. Abshaev, R. Bruintjes, M. Murakami, T. Prabhakaran, and Z. Yao, 2019: Review of advances in precipitation enhancement research. *Bull. Amer. Meteor. Soc.*, **100**, 1465-1480.

Fujibe, F., M. Murakami, T. Koshida, and K. Yoshida, 2008: Climatology of precipitation variability over the Sameura dam catchment and its relation to the dam water storage. *TENKI*, **55**, 469-473 (in Japanese).

Geresdi, I., L. Xue, S. Chen, Y. Wehbe, R. Bruintjes, J. A. Lee, R. M. Rasmussen, W. W. Grabowski, N. Sarkadi, and S. A. Tessendorf, 2021: Impact of hygroscopic seeding on the initiation of precipitation formation: Results of a hybrid bin microphysics parcel model. *Atmos. Chem. Phys.*, **21**, 16143-16159.

Koshida, T., M. Murakami, K. Yoshida, F. Fujibe, and K. Takahashi, 2012: Assessment of clouds suitable for summertime precipitation augmentation over Shikoku Island. *SOLA*, **8**, 160-164, doi:10.2151/sola.2012-039.

Kuba, N., and M. Murakami, 2010: Effect of hygroscopic seeding on warm rain clouds – Numerical study using a hybrid cloud microphysical model. *Atmos. Chem. Phys.*, **10**, 3335-3351, doi:10.5194/acp-10-3335-2010.

Kuba, N., and M. Murakami, 2012: Effect of hygroscopic seeding on warm rain clouds - Numerical study using a hybrid cloud microphysical model. *Proceedings of the Sixteenth International Conference on Clouds and Precipitation*, 10.2-1, Leipzig, Germany.

Mather, G. K., D. E. Terblanche, F. E. Steffens, and L. Fletcher, 1997: Results of the South African cloud-seeding experiments using hygroscopic flares. *J. Appl. Meteor.*, **36**, 1433-1447.

Misumi, R., A. Hashimoto, M. Murakami, N. Kuba, N. Orikasa, A. Saito, T. Tajiri, K. Yamashita, and J. P. Chen, 2010: Microphysical structure of a developing convective snow cloud simulated by an improved version of the multi-dimensional bin model. *Atmos. Sci. Let.*, **11**, 186-191.

Murakami, M., and JCSEPA research group, 2011: Japanese Cloud Seeding

Experiments for Precipitation Augmentation (JCSEPA) – New approaches and some results from wintertime and summertime weather modification programs. *10th WMP Scientific Conference on Weather Modification*, Bali, Indonesia, 4-7 October 2011.

Murakami, M., F. Fujibe, and M. Ishihara, 2015: Frontier of weather modification research. *Meteorological Research Note*, Meteorological Society of Japan, 340 pp (in Japanese).

Petters, M. D., and S. M. Kreidenweis, 2007: A single parameter representation of hygroscopic growth and cloud condensation nucleus activity. *Atmos. Chem. Phys.*, **7**, 1961-1971, doi:10.5194/acp-7-1961-2007.

Reisin T., S. Tzivion, and Z. Levin, 1996: Seeding convective clouds with ice nuclei or hygroscopic particles: A numerical study using a model with detailed microphysics. *J. Appl. Meteor.*, **35**, 1416-1434.

Rosenfeld, D., D. Axisa, W. L. Woodley, and R. Lahav, 2010: A quest for effective hygroscopic cloud seeding. *J. Appl. Meteorol. Climatol.*, **49**, 1548-1562.

Segal, Y., A. Khain, M. Pinsky, and D. Rosenfeld, 2004: Effects of hygroscopic seeding on raindrop formation as seen from simulations using a 2000-bin spectral cloud parcel model. *Atmos. Res.*, **71**, 3-34.

Silverman, B. A., and W. Sukarnjanaset, 2000: Results of the Thailand warm-cloud hygroscopic particle seeding experiment. *J. Appl. Meteor.*, **39**, 1160-1175.

Tajiri, T., N. Orikasa, Y. Zaizen, T.-H. Kuo, W.-C. Kuo, and M. Murakami, 2020. CCN and INP abilities of hybrid flare particles measured with MRI continuous-flow diffusion chamber-type IN counter and MRI cloud simulation chamber, *The 22nd AMS Conference on Planned and Inadvertent Weather Modification*, 5-2, Boston, Massachusetts, USA, January 12-16, 2020.

Terblanche, D. E., F. E. Steffens, L. Fletcher, M. P. Mittermaier, and R. C. Parsons, 2000: Toward the operational application of hygroscopic flares for rainfall enhancement in South Africa. *J. Appl. Meteor.*, **39**, 1811-1821.

Tessendorf, S. A., S. Chen, C. Weeks, R. Bruintjes, R. M. Rasmussen, and L. Xue, 2021: The influence of hygroscopic flare seeding on drop size distribution over southeast Queensland. *JGR Atmospheres*, **126**, 1-15.

Yamashita, K., M. Murakami, A. Hashimoto, and T. Tajiri, 2011: CCN ability of Asian mineral dust particles and their effects on cloud droplet formation. *J. Meteor. Soc. Jpn*, **89**, 581-587.

Yamashita, K., W.-C. Kuo, M. Murakami, T. Tajiri, A. Saito, N. Orikasa, and H. Ohtake, 2023: Physical properties of background aerosols and CCN measured in Kochi city in June 2010 and its implication for planned and inadvertent cloud modification. *J. Meteor. Soc. Jpn* (submitted).

Yin, Y., Z. Levin, T. G. Reisin, and S. Tzivion, 2000: Seeding convective clouds with hygroscopic flares: Numerical simulations using a cloud model with detailed microphysics. *J. Appl. Meteor*., **39**, 1460-1472.

WMO, 2000: Report of the WMO International workshop on hygroscopic seeding: Experimental results, physical processes, and research needs. WMP Report No. 35, World Meteorological Organization, Geneva Switzerland, 68 pp.

List of Figures

Fig. 1 Median (red dashed line), 90th (blue dashed line), and 10th (green dashed line) percentile size distributions of background APs measured using scanning mobility particle sizer (SMPS) and optical particle counter (OPC) in Kochi city and their log-normal fits (solid lines). The three particle size distributions show the median, 90th percentile, and 10th percentile of the number concentration for each particle size.

Fig. 2 Number size distributions of MP and HF particles measured by SMPS, OPC, cloud aerosol spectrometer (CAS), and forward scattering spectrometer probe (FSSP) on board an instrumented aircraft flying approximately 1 km behind a seeding helicopter and their approximations by multiple log-normal distributions shown by solid lines (upper) and multiple log-normal approximations of number (black) and mass (red) size distributions (lower). The size distributions of MP and HF are with BG aerosol subtracted.

Fig. 3 Bimodal size distribution of APs with hygroscopicity of 0.1 (black line) and the shifted one toward smaller sizes to have mode sizes corresponding to the same critical supersaturations for APs with hygroscopicity of 1.2 (red line).

Fig. 4 Droplet size distributions after (a) 20 s and (b) 200 s from the activation point obtained from the model simulation. The legend presents the hygroscopicity and size distributions shown in Fig. 3 used in the simulation.

Fig. 5 Size distributions of aerosol particles (APs) and cloud droplets. (a) Initial size distributions of dry BG APs with seeding aerosols and droplet size distributions at (b) 500 m and (c) 600 m obtained from the model simulation using the initial size distribution of BG and seeding aerosols shown in (a) and updraft velocity of 1.0 m s^{-1} for the MP case.

Fig. 6 Time series of (a) relative humidity and (b) CN (solid line), droplet (dashed line), and raindrop (dash-dotted line) number concentrations obtained from the model simulations for the same case shown in Fig. 5. In the lower panel, the left axis is for CN and droplet number concentrations, and the right axis is for raindrop concentration.

Fig. 7 The production rate of (a) the number and (b) mass of raindrops via collision–coalescence (blue) and condensational (red) growth for BG + MP case.

Fig. 8 Same as Fig. 5, but for the HF case.

Fig. 9 Same as Fig. 6, but for the HF case.

Fig. 10 Same as Fig. 7, but for BG + HF case.

List of Tables

Table 1 Parameters for size bin setup. q_i is the bin-sizing factor used in the equation to determine the lower bin limits of successive larger mass bins from i = 3 through i = N-1, while θ is a coefficient to determine the change in the bin-sizing factor. Please see the equations in the text.

Table 2 Seeding aerosol amount dependency of MP and HF seeding effects at updraft velocity of 1.0 m s^{-1} for three different BG AP size distributions. The value at the top of each row indicates the maximum cloud droplet

number concentration during the simulation period, and the value in parentheses at the bottom indicates the ratio to the maximum cloud droplet number concentration without seeding.

Table 3 BG AP hygroscopicity dependence of MP and HF seeding effects at updraft velocity of 1.0 m s^{-1} for three different BG AP size distributions

Table 4 Updraft velocity dependence of MP and HF seeding effects for three different BG AP size distributions

Table 5 Effect of anti-caking agent on MP seeding effect at updraft velocity of 1.0 m s^{-1} for three different BG AP size distributions

Table 6 HF particle's physicochemical property dependence of seeding effect at updraft velocity of 1.0 m s^{-1} for three different BG AP size distributions

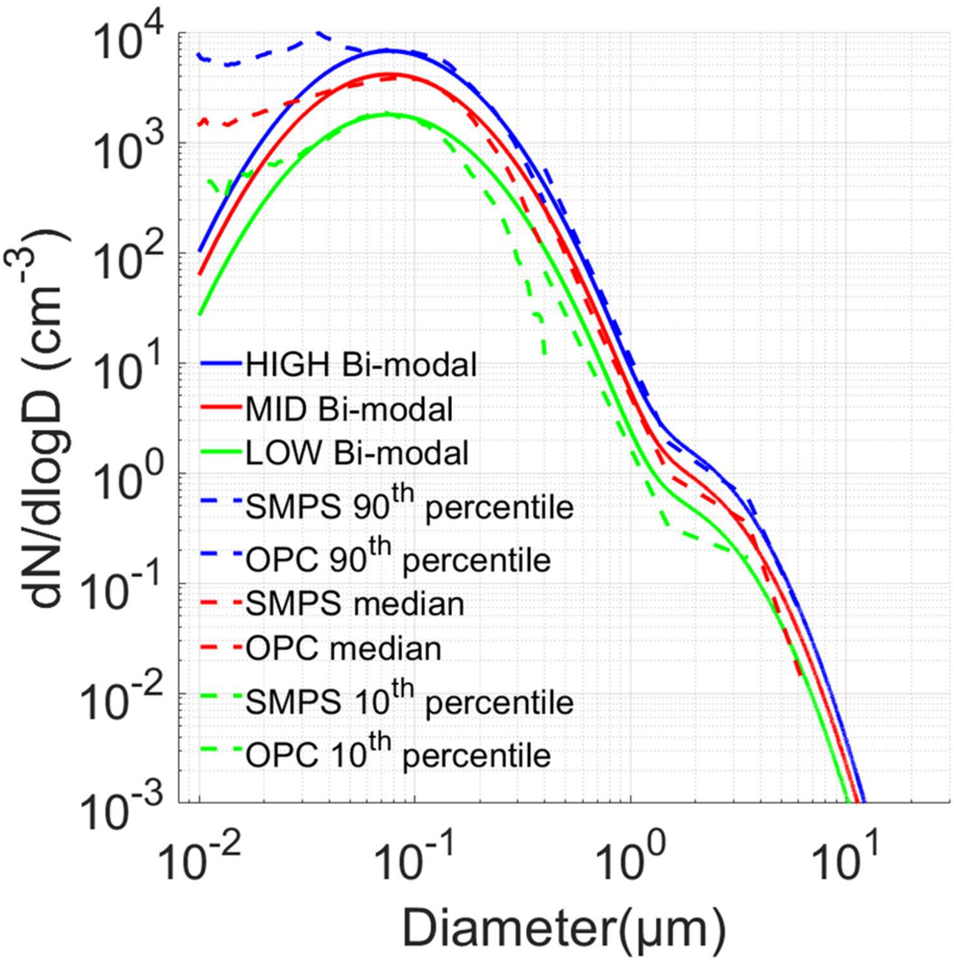

Fig. 1 Median (red dashed line), 90th (blue dashed line), and 10th (green dashed line) percentile size distributions of background APs measured using scanning mobility particle sizer (SMPS) and optical particle counter (OPC) in Kochi city and their log-normal fits (solid lines). The three particle size distributions show the median, 90th percentile, and 10th percentile of the number concentration for each particle size.

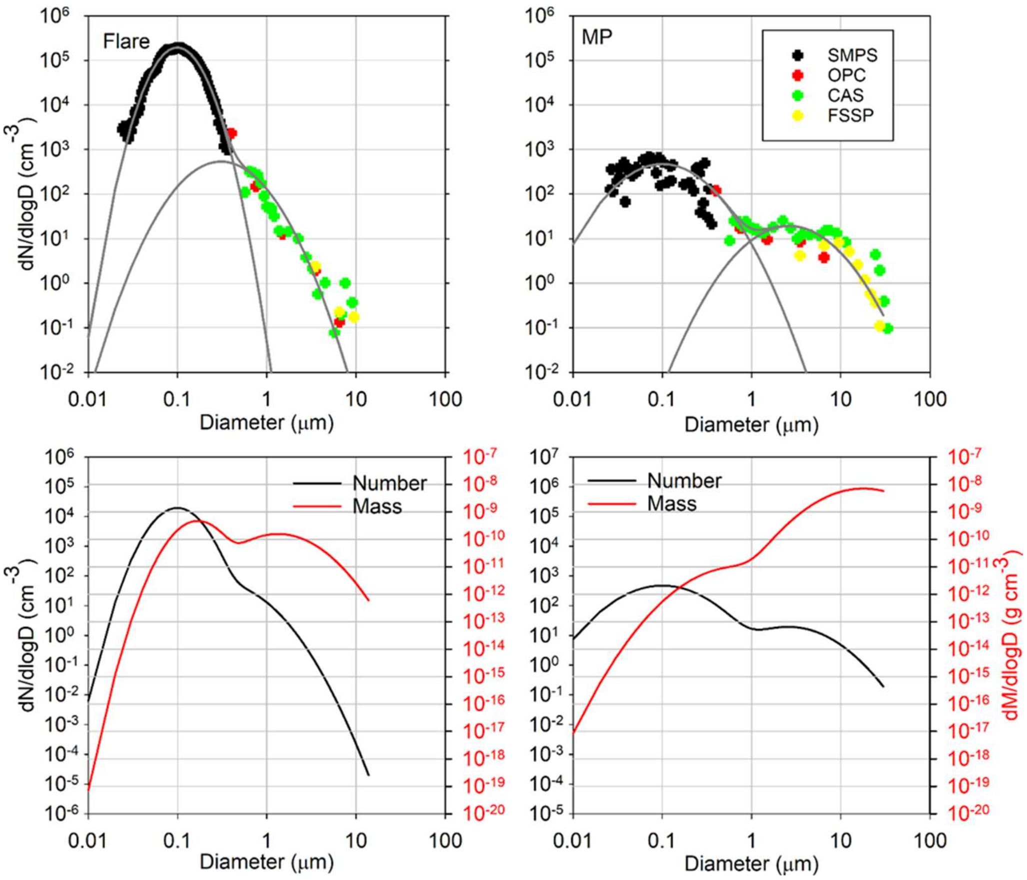

Fig. 2 Number size distributions of MP and HF particles measured by SMPS, OPC, cloud aerosol spectrometer (CAS), and forward scattering spectrometer probe (FSSP) on board an instrumented aircraft flying approximately 1 km behind a seeding helicopter and their approximations by multiple log-normal distributions shown by solid lines (upper) and multiple log-normal approximations of number (black) and mass (red) size distributions (lower). The size distributions of MP and HF are with BG aerosol subtracted.

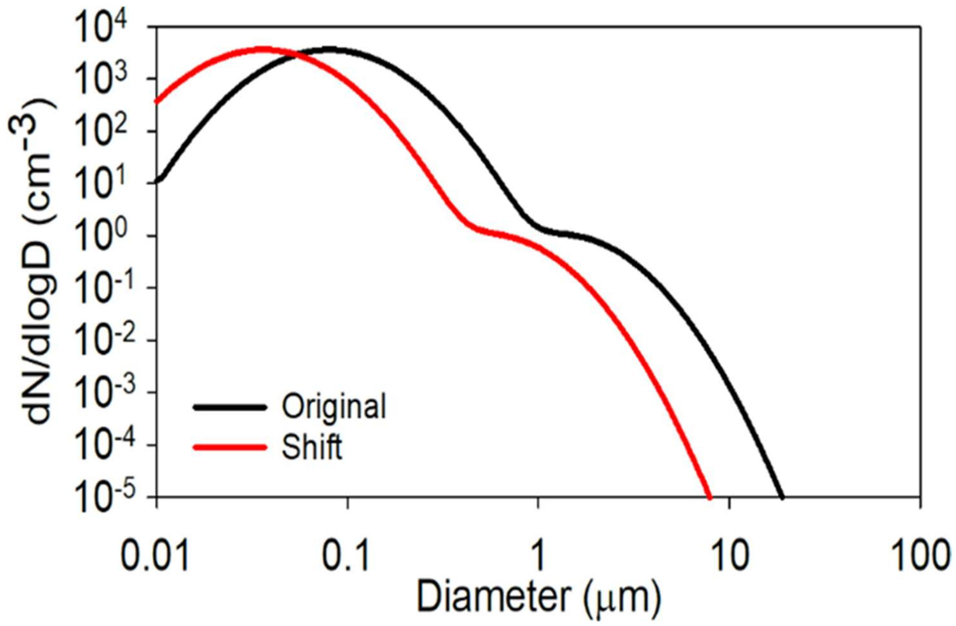

Fig. 3 Bimodal size distribution of APs with hygroscopicity of 0.1 (black line) and the shifted one toward smaller sizes to have mode sizes corresponding to the same critical supersaturations for APs with hygroscopicity of 1.2 (red line).

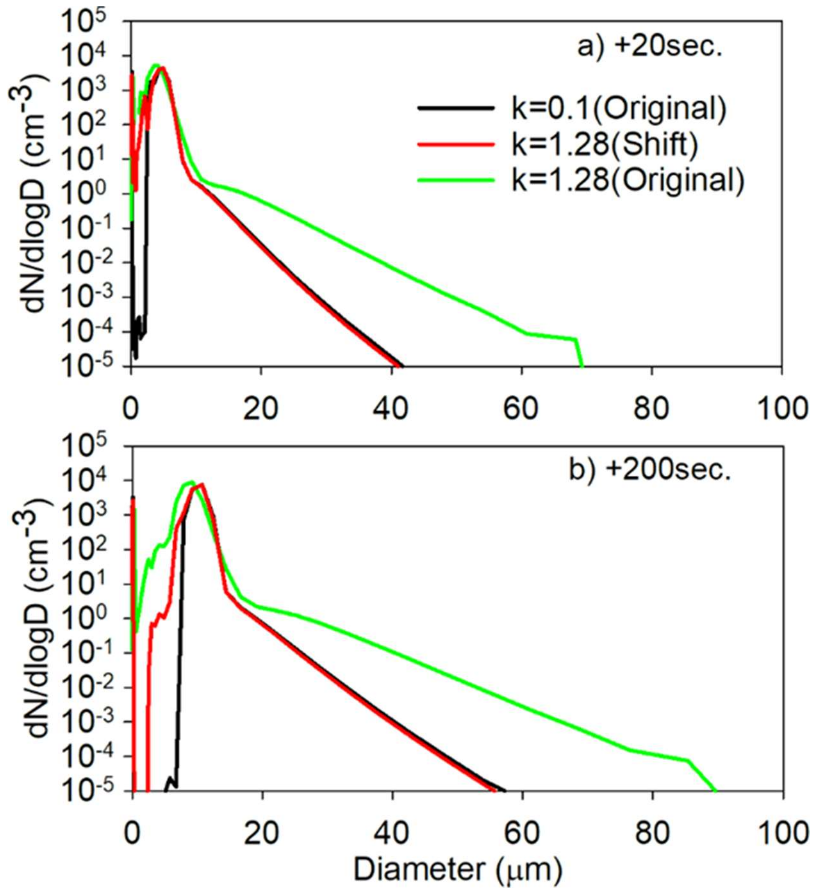

Fig. 4 Droplet size distributions after (a) 20 s and (b) 200 s from the activation point obtained from the model simulation. The legend presents the hygroscopicity and size distributions shown in Fig. 3 used in the simulation.

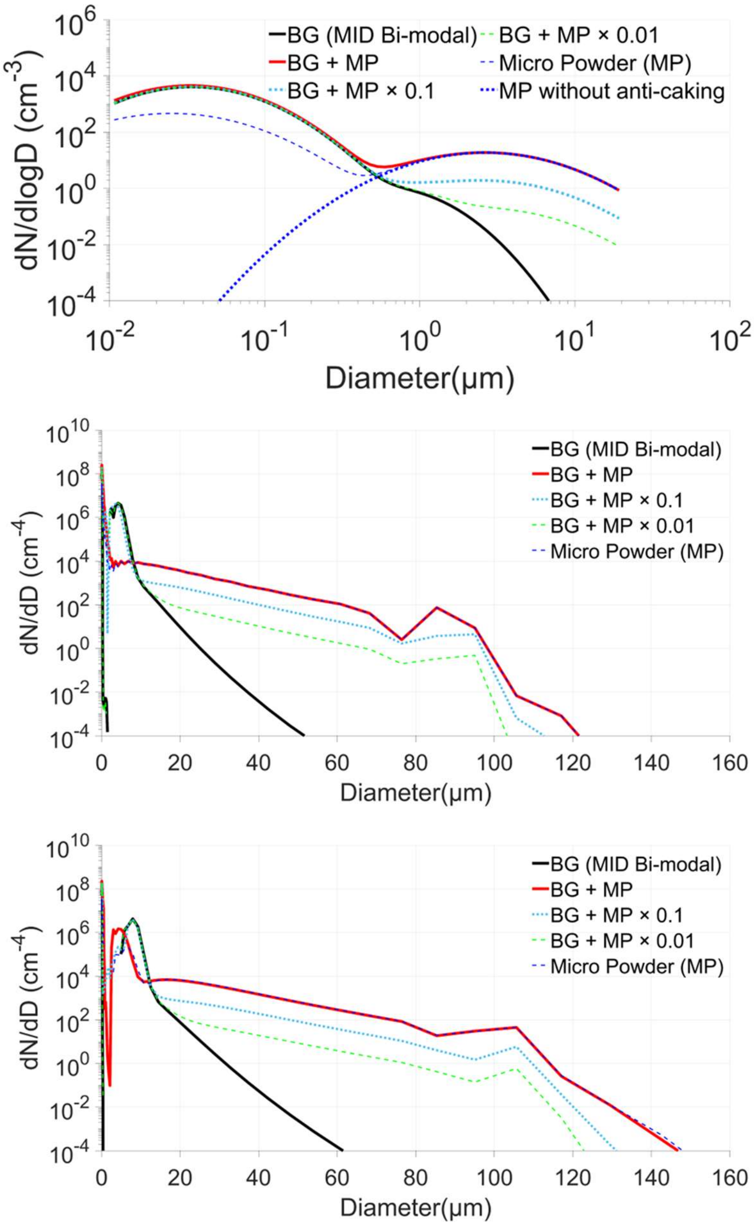

Fig. 5 Size distributions of APs and cloud droplets. (a) Initial size distributions of dry BG APs with seeding aerosols and droplet size distributions at (b) 500 m and (c) 600 m obtained from the model simulation using the initial size distribution of BG and seeding aerosols shown in (a) and updraft velocity of 1.0 m s^{-1} for the MP case.

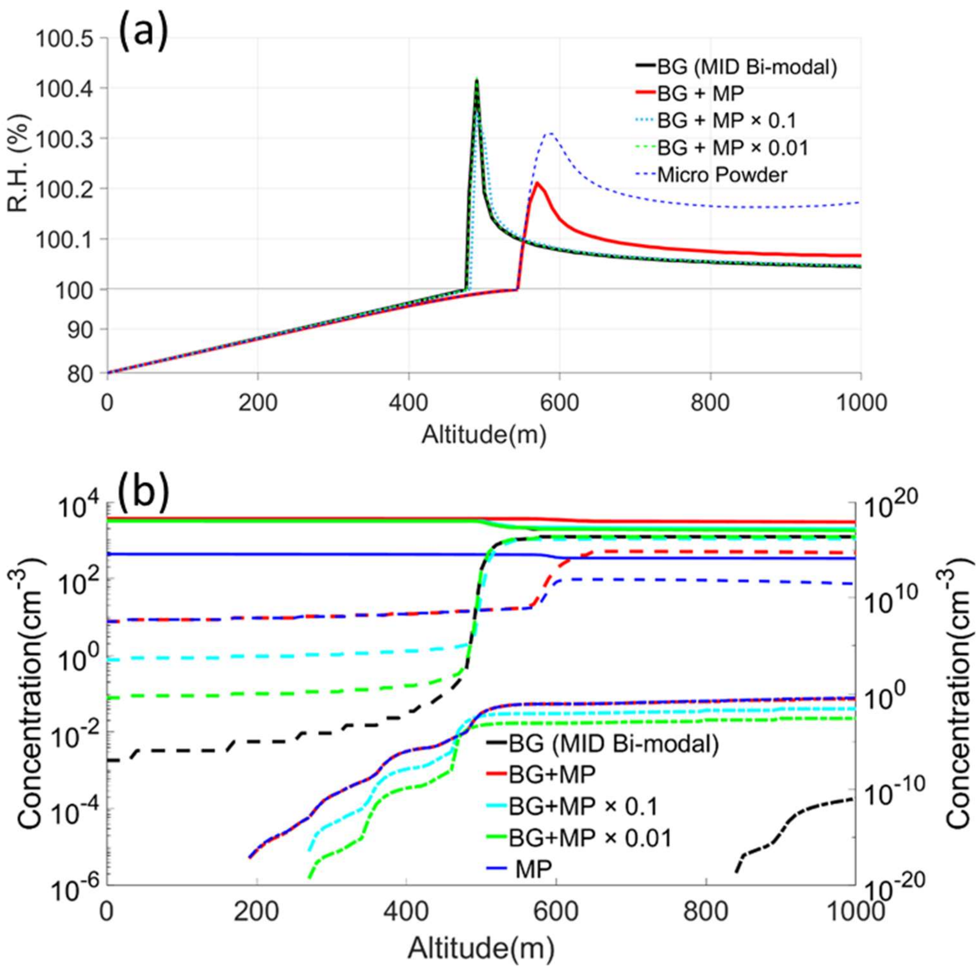

Fig. 6 Time series of (a) relative humidity and (b) CN (solid line), droplet (dashed line), and raindrop (dash-dotted line) number concentrations obtained from the model simulations for the same case shown in Fig. 5. In the lower panel, the left axis is for CN and droplet number concentrations, and the right axis is for raindrop concentration.

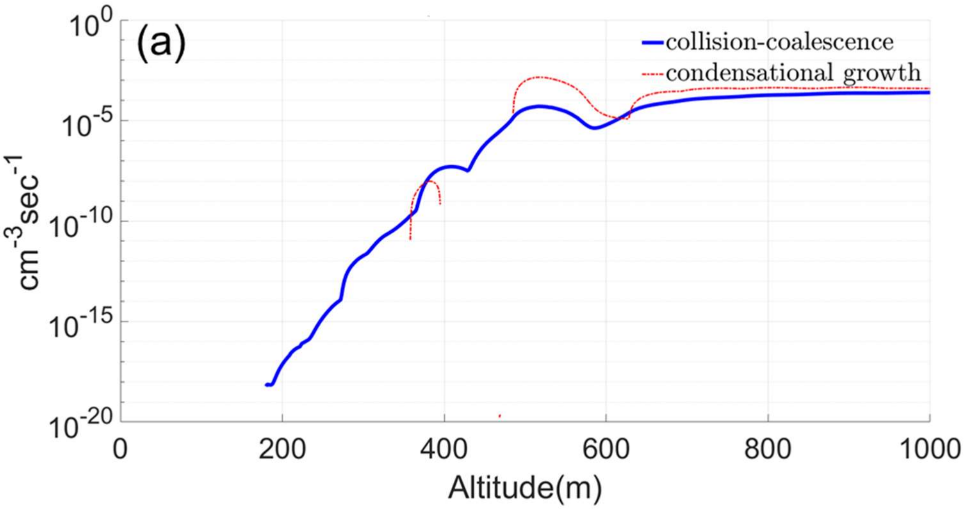

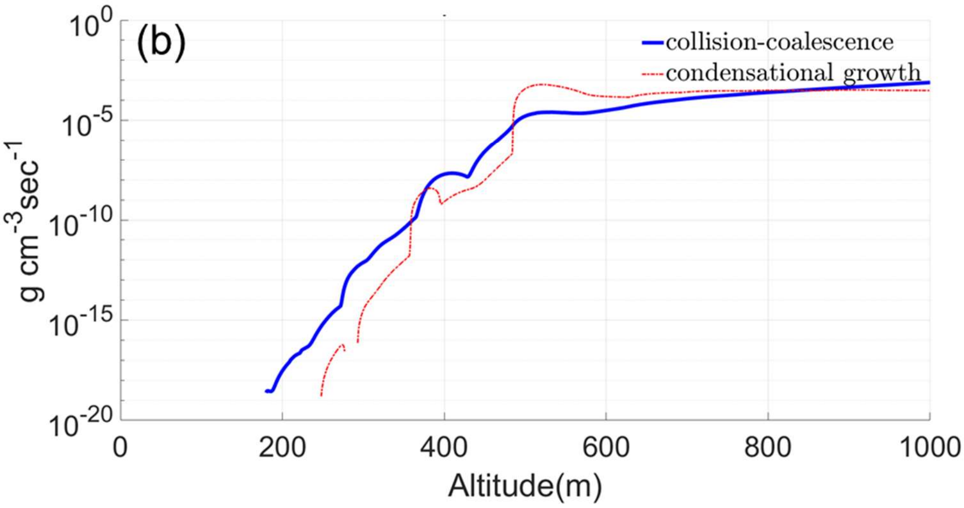

Fig. 7 The production rate of (a) the number and (b) mass of raindrops via collision-coalescence (blue) and condensation (red) growth for BG + MP case

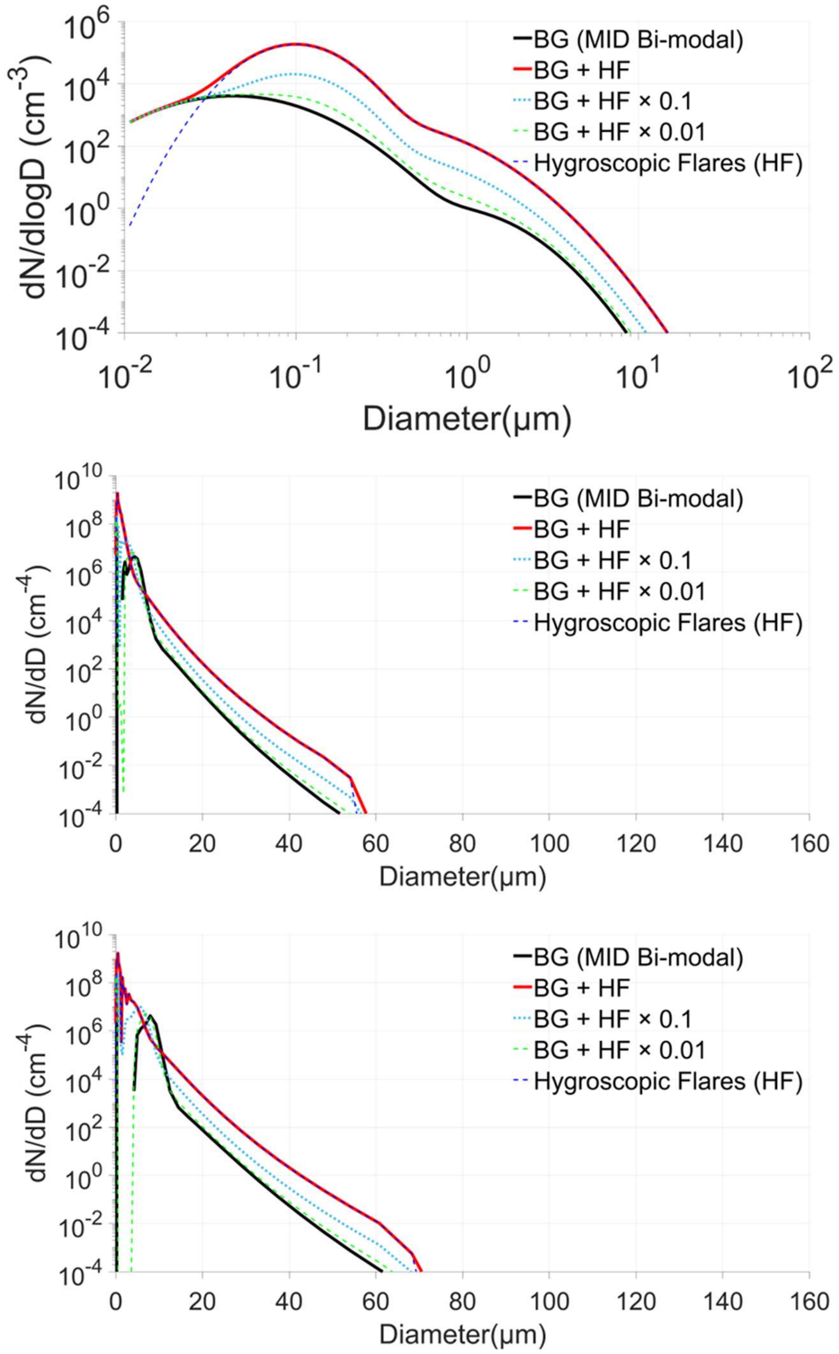

Fig. 8 Same as Fig. 5, but for the HF case.

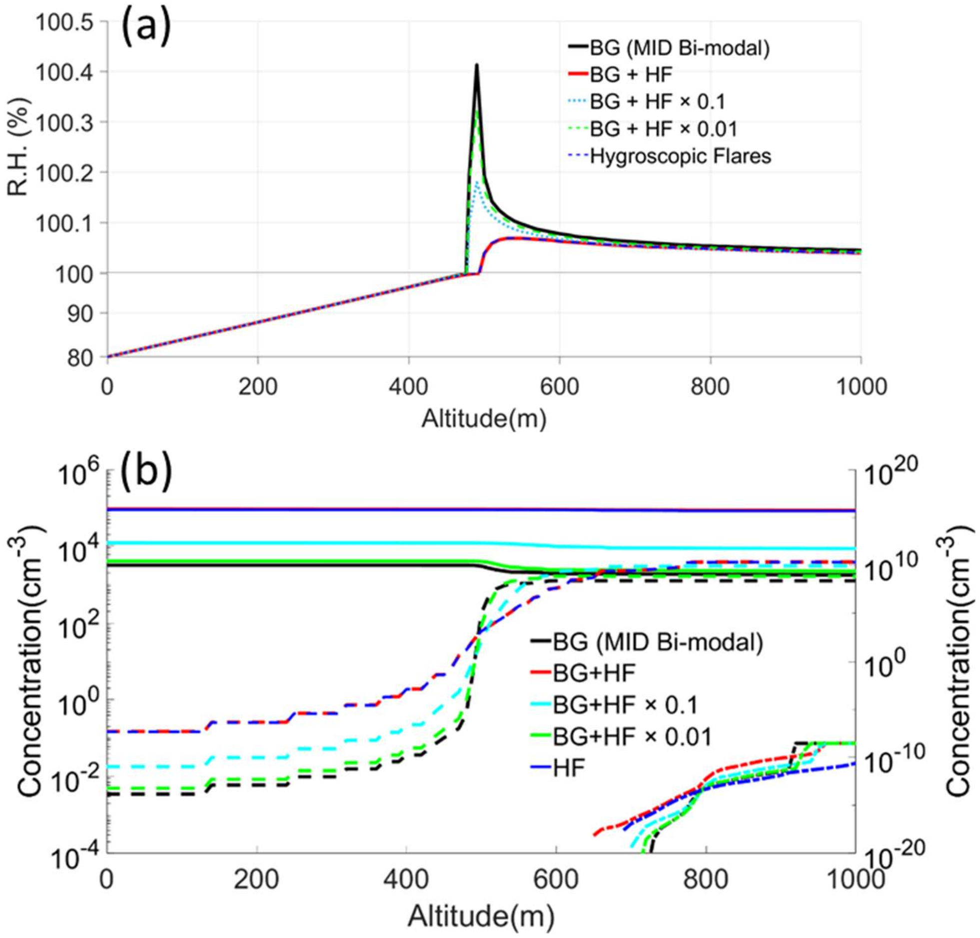

Fig. 9 Same as Fig. 6, but for the HF case.

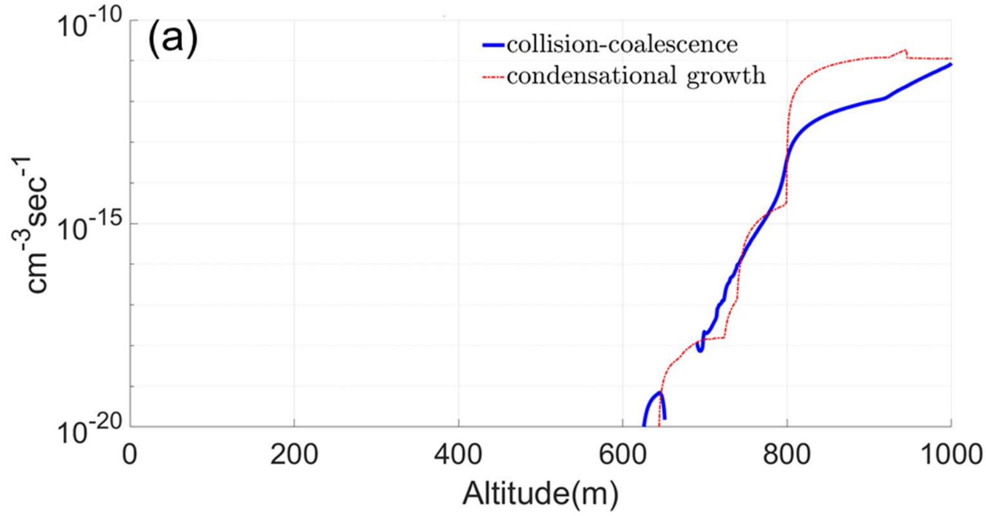

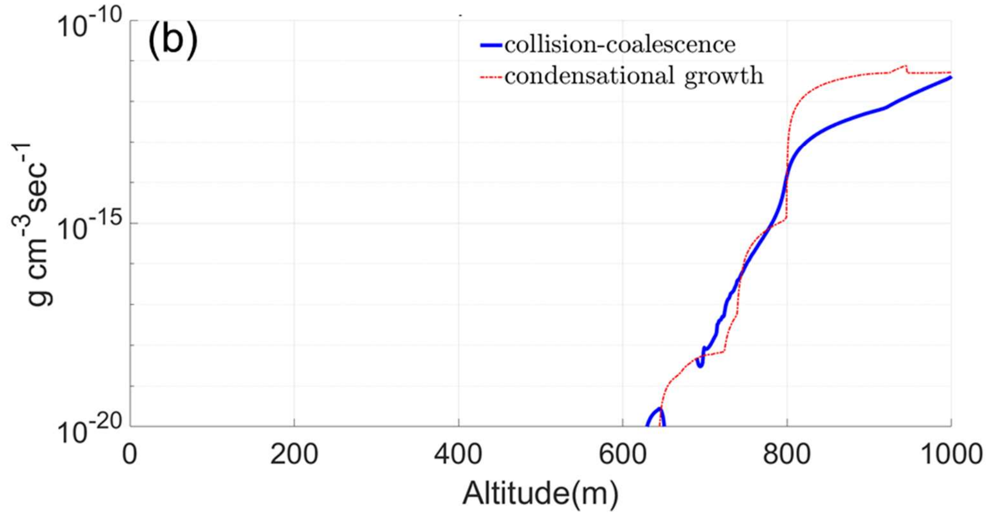

Fig. 10 Same as Fig. 7, but for BG + HF case.

Table 1 Parameters for size bin setup. q_i is the bin-sizing factor used in the equation to determine the lower bin limits of successive larger mass bins from i=3 through i=N-1, while θ is a coefficient to determine the change in the bin-sizing factor. Please see the equations in the text.

	Number of bins N	$\mathbf{q_2}$	θ	m_1 (kg) r_1 (m)	m_2 (kg) r_2 (m)	m_N (kg) r_N (m)	m_{N+1} (kg) r_{N+1} (m)
Water	72	1.385	1.000	4.192e-26 (2.155e-10)	5.353e-21 (1.085e-8)	6.431e-8 (2.485e-4)	7.548e-8 (2.622e-4)
Aerosol	72	2.0	1.008	9.792e-25 (5.093e-10)	9.652e-22 (5.069e-9)	7.833e-12 (1.019e-5)	1.321e-4 (2.613e-3)

Table 2 Seeding aerosol amount dependency of MP and HF seeding effects at updraft velocity of 1.0 m s^{-1} for three different BG AP size distributions. The value at the top of each row indicates the maximum cloud droplet number concentration during the simulation period, and the value in parentheses at the bottom indicates the ratio to the maximum cloud droplet number concentration without seeding.

Max. Droplet Conc. (cm^{-3}) (Conc. Ratio)	LOW Bi-modal	MID Bi-modal	HIGH Bi-modal
BG + MP	318 (0.51)	516 (0.42)	628 (0.37)
BG + MPx0.1	625 (1.01)	1099 (0.89)	1441 (0.84)
BG + MPx0.01	616 (1.00)	1236 (1.00)	1712 (1.00)
BG + HF	3872 (6.19)	3893 (3.09)	3916 (2.30)
BG + HFx0.1	3034 (4.85)	3070 (2.44)	3068 (1.80)
BG + HFx0.01	1266 (2.02)	1656 (1.32)	1902 (1.12)

Table 3 BG AP hygroscopicity dependence of MP and HF seeding effects at updraft velocity of 1.0 m s^{-1} for three different BG AP size distributions.

Max. Droplet Conc. (cm^{-3}) (Conc. Ratio)	BG κ=0.03	BG κ=0.1	BG κ=0.3
LOW + MP	234 (0.52)	318 (0.51)	450 (0.56)
MID + MP	353 (0.40)	516 (0.45)	661 (0.45)
HIGH + MP	508 (0.42)	628 (0.41)	818 (0.42)
LOW + HF	3861 (8.37)	3872 (6.19)	3908 (4.81)
MID + HF	3867 (4.31)	3893 (3.09)	3975 (2.66)
HIGH + HF	3873 (3.22)	3916 (2.30)	4050 (2.14)

Table 4 Updraft velocity dependence of MP and HF seeding effects for three different BG AP size distributions.

Max Droplet Conc. (cm^{-3}) (Conc. Ratio)	w=0.5 m s^{-1}	w=1.0 m s^{-1}	w=2.0 m s^{-1}
LOW + MP	115 (0.26)	318 (0.51)	711 (0.91)
MID + MP	173 (0.21)	516 (0.42)	1183 (0.73)
HIGH + MP	194 (0.20)	628 (0.37)	1688 (0.72)
LOW + HF	2299 (4.98)	3872 (6.19)	6303 (7.93)
MID + HF	2312 (3.00)	3893 (3.09)	6334 (3.83)
HIGH + HF	2328 (2.39)	3916 (2.30)	6367 (2.69)

Table 5 Effect of anti-caking agent on MP seeding effect at updraft velocity of 1.0 m s^{-1} for three different BG AP size distributions.

Max. droplet conc. (cm^{-3}) (Conc. Ratio)	w/ anti-caking agent	w/o anti-caking agent
LOW Bi-modal + MP	318 (0.51)	295 (0.48)
MID Bi-modal + MP	516 (0.42)	474 (0.38)
HIGH Bi-modal + MP	628 (0.37)	614 (0.36)

Table 6 HF particle's physicochemical property dependence of seeding effect at updraft velocity of 1.0 m s^{-1} for three different BG AP size distributions.

Max. Droplet Conc. (cm^{-3}) (Conc. ratio)	HF κ=0.6 1st mode dia.=0.3 μm	HF κ=1.1 1st mode dia.=0.3 μm	HF κ=0.6 No 2nd mode 1st mode dia.=0.3 μm	HF κ=0.6 No 2nd mode 1st mode dia.=0.5 μm	HF κ=0.6 No 2nd mode 1st mode dia.=1.0 μm	HF κ=0.6 No 2nd mode 1st mode dia.=2.0 μm
LOW Bi-modal + HF	3872 (6.19)	3867 (6.07)	674 (1.08)	496 (0.79)	389 (0.62)	339 (0.54)
MID Bi-modal + HF	3893 (3.10)	3876 (3.21)	1000 (0.79)	615 (0.49)	392 (0.31)	339 (0.27)
HIGH Bi-modal + HF	3916 (2.31)	3887 (2.44)	1169 (0.69)	712 (0.42)	396 (0.23)	340 (0.20)